Do Feature Attribution Methods Correctly Attribute Features?

Yilun Zhou[1]   **Serena Booth**[1]   **Marco Tulio Ribeiro**[2]   **Julie Shah**[1]

[1]MIT CSAIL   [2]Microsoft Research
{yilun, serenabooth, julie_a_shah}@csail.mit.edu
marcotcr@microsoft.com

Abstract

Feature attribution methods are exceedingly popular in interpretable machine learning. They aim to compute the attribution of each input feature to represent its importance, but there is no consensus on the definition of "attribution", leading to many competing methods with little systematic evaluation. The lack of attribution ground truth further complicates evaluation, which has to rely on proxy metrics. To address this, we propose a dataset modification procedure such that models trained on the new dataset have ground truth attribution available. We evaluate three methods: saliency maps, rationales, and attention. We identify their deficiencies and add a new perspective to the growing body of evidence questioning their correctness and reliability in the wild. Our evaluation approach is model-agnostic and can be used to assess future feature attribution method proposals as well. Code is available at `https://github.com/YilunZhou/feature-attribution-evaluation`.

1 Introduction

Consider the task of training a neural network to detect cancers from X-ray images. The data come from two sources, a general hospital and a specialized cancer center. Images from the cancer center contain many more cancer cases. Furthermore, the cancer center adds a small timestamp watermark to the top-left corner of its images. As the result, the watermark presence may affect model prediction—after all, it is a strong predictor of a cancer diagnosis.

It is important to ensure the deployed model makes predictions based on genuine medical signals rather than image artifacts such as the watermark. If these artifacts are known *a priori*, we can evaluate the model on counterfactual pairs—images with and without them—and look for difference in prediction to assess their impact. Realistically, however, for almost all datasets in the wild we cannot anticipate every possible artifact. In this case, feature attribution methods such as saliency maps [4, 17, 21, 24, 27, 28] are used to identify regions most important to the prediction, which are then inspected for evidence of any potential artifacts, e.g. the watermark. Such a train-and-interpret pipeline has been widely adopted in data-driven medical diagnosis studies [19, 25, 26].

Crucially, the above assessment depends on the feature attribution methods working correctly and not missing any features that are influential to the model. Is this truly the case? Direct evaluation on natural datasets is impossible as the very spurious correlations we want attribution methods to find are, by definition, unknown. Current evaluations try to sidestep this problem with proxy metrics [6, 11, 23], which unfortunately are limited in various ways by the lack of ground truth (see Sec. 2.2).

We instead propose evaluating these methods on *semi-natural* datasets: natural datasets modified with well-defined manipulations. This modification (Fig. 1) ensures that *any* classifier with sufficiently high performance has to rely, sometimes solely, on features resulting from certain manipulation. We then present desiderata, or necessary conditions, for the the correct attribution values given this ground truth; for example, features known to not affect the model's decision should not be highlighted.

Our dataset-based evaluation is agnostic to both the model and the attribution method. In experiments, we evaluate saliency maps, rationale models, and attention mechanisms and identify several failures. We discuss potential reasons for such failures and recommend directions of remedy.
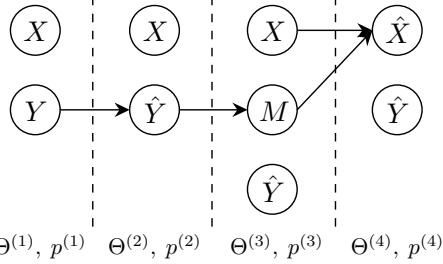
Figure 1: Our proposed the dataset modification procedure, which constructs a ground truth for feature attribution. Arrows indicate modifications. (1) A model $\Theta^{(1)}$ trained on a dataset (X, Y) achieves a generalization accuracy of $p^{(1)}$. Without further knowledge, the best upper bound on $p^{(1)}$ is perfect performance of 1. (2) We modify the label Y to $\hat{Y}$, where $\hat{Y}$ is a (more) stochastic version of Y. Now we can bound the accuracy $p^{(2)}$ of model $\Theta^{(2)}$ by $p^* < 1$. (3) We introduce a manipulation M, which can be abstractly represented as e.g. a binary variable, conditioned on $\hat{Y}$. For some $p(M|\hat{Y})$, a model $\Theta^{(3)}$ trained on the augmented input (X, M) can achieve an accuracy $p^{(3)} > p^*$. *If so, it is guaranteed that the model has to use M.* (4) We modify X according to M to get $\hat{X}$, so that we can explain model $\Theta^{(4)}$ with existing attribution methods. For example, for a watermarking manipulation M, $\hat{X}$ is a watermarked version of image X if $M = 1$, and X if $M = 0$.

2 Related Work

2.1 Feature Attribution Methods

Feature attribution methods assign attribution scores to input features, the absolute value of which informally represents their importance to the model prediction or performance. **Saliency maps** explain an image I by producing S of the same size, where $S_{h,w}$ indicates the contribution of pixel $I_{h,w}$, which has been interpreted as sensitivity [27], relevance [4], local influence [21], Shapley values [17], or filter activations [24]. **Attention mechanisms** [5] were originally proposed to better retain sequential information. Recently they have been used as attribution values, but their their validity is under debate with different and inconsistent criteria being proposed [13, 20, 30]. **Rationale models** [6, 14, 16] are inherently interpretable models for text classification with a two-stage pipeline: a selector extracts a rationale (i.e. input words), and a classifier makes a prediction based on it. The selected rationales are often regularized to be succinct and continuous.

2.2 Evaluation of Feature Attributions

A popular way to evaluate attributions is to assess alignment with human judgment, but models and humans can reach the same prediction while using entirely different reasoning mechanisms (e.g. medical signals used by doctors and watermarks used by the model). For example, Smilkov et al. [28] proposed SmoothGrad as a better alternative to the vanilla Gradient method [27]. They showed this method to be less noisy, but did not investigate whether attribution values *should* be smooth. Bastings et al. [6] evaluated their rationale model by assessing its agreement with human rationale annotation, but a model may achieve high accuracy with subtle but strongly correlated textual features such as grammatical idiosyncrasy. Covert et al. [8] compared the feature attribution of a cancer prediction model to scientific knowledge, yet even a well-performing model may rely on other signals.

Another common approach successively removes features with highest attribution values and evaluates certain metrics. The first metric is model prediction change [e.g. 3, 12, 23]. These evaluations do not account for nonlinear interactions. For example, if the model learns an OR function of two features and both are active in an instance, the evaluation will (incorrectly) deem whichever feature removed first to be useless as its removal does not affect the prediction. The second metric is model retraining performance [11]. It fails when the retrained model can rely on different features while still achieving the same accuracy. For example, a model might achieve some accuracy by using only feature x_1. If a retrained model using only x_2 achieves the same accuracy, the evaluation framework would (falsely) reject the ground truth attribution on x_1 due to the same re-training accuracy.

Most similar to our proposal are works that also construct semi-natural datasets with explicitly defined ground truth explanation [2, 31]. Adebayo et al. [2] used a perfect background correlation for a dog-vs-bird dataset, verified that the model achieves high accuracy on background alone, thus

claiming that the correct attribution should focus solely on the background. However, we verified that a model on their dataset can achieve high accuracy *simultaneously* on foreground alone, background alone, and both combined, invalidating their claimed ground truth. Similarly, Yang and Kim [31] argues that for *background* classification, a more label-correlated foreground should receive higher attribution value. However, since in their dataset, the background labels are not changed, a model could still rely solely on background pixels regardless of foreground correlation. We avoid these pitfalls through label reassignment in Sec. 4, which forces the model to use certain features in order to achieve high accuracy. Furthermore, they also share another subtle failure mode, which we elaborate in the Remark at the end of Sec. 4 after formalizing our approach.

Finally, Adebayo et al. [1] proposed sanity checks for saliency maps by assessing their change under weight or label randomization. We establish complementary necessary conditions for good explanations by instead focusing on model-agnostic dataset-side modifications. We show that even methods which pass their randomization tests do not perform well on our evaluations.

3 Desiderata for Attribution Values

What should the attribution value be? Even though precise values may be axiomatic, there are certain properties that are *de facto* requirements if we want people to understand how a model makes a decision, verify that reasoning process is sound, and possibly inform options for correction if it is not (c.f. the opening example in Sec. 1). For example, while LIME and SHAP define attribution scores differently, both explanations are bad if they highlight features completely ignored by the model.

We study two types of features: those of fundamental importance to the model, denoted by F_C, and those non-informative to the label, denoted by F_N. The first requirement is that it should not miss important features F_C. Unfortunately, identifying all such features is not easy. For example, while the model could use the timestamp on some X-ray images for cancer prediction, it could also exclusively rely on genuine medical features (as done by human doctors), and attributions should only highlight the timestamp in the former case. This is the central goal of our proposed dataset modification procedure detailed in the next section. Briefly, we can modify the dataset in such a way that using only medical features could not achieve a high accuracy due to label noise, and thus establishing the ground truth usage of the timestamp for any model with high performance. We can then evaluate how well the attribution method identifies the contribution of the timestamp by the attribution percentage $\text{Attr}\%$ of the timestamp pixels, with $\text{Attr}\%(F) \doteq \left(\sum_{i \in F} |s_i| \right) / \left(\sum_{i=1}^{D} |s_i| \right)$, where D is the total number of features and s_i is the attribution value assigned to the i-th feature.

Conversely, we can introduce non-informative features F_N independent from the label, such as a white border added to a random subset of images. They do not and cannot contribute to the model performance, and we should expect $\text{Attr}\% = 0$ on them from any method that analyzes features contributing to the a high model performance. In addition, as the model performance increases, the model prediction is less and less "distracted" by these features, resulting in $\text{Attr}\% \to 0$.

While the above criteria work well for evaluating *post-hoc* explanations, inherently interpretable models, such as text rationale models, produce correct-by-definition explanations. However, not all explanations are created equal. For example, one explanation comprehensively and exclusively selects important features F_C, while another barely selects F_C but highlights lots of non-informative features F_N. Although both allow for highly accurate predictions, the former is much easier for humans to understand, while the latter obfuscates the model reasoning with unnecessary information.

Many inherently interpretable models work by classifying on an (input-dependent) set of sparse features F, which naturally become the explanation. To capture the intuition described above, we define two metrics, precision and recall, defined as $\text{Pr}(F) = |F \cap F_C|/|F|$, and $\text{Re}(F) = |F \cap F_C|/|F_C|$. The ideal model should have one of them to be 1.

4 Dataset Modification

We now present the dataset modification procedure that lets us quantify the influence of certain features to the model. We use a running example of adding a watermark pattern to an X-ray cancer dataset without any watermark, such that the watermark is guaranteed to affect the model decision.

Setup   Let $\mathcal{X}$ and $\mathcal{Y} \doteq \{1, ..., K\}$ be the input and output space for K-class classification, jointly distributed as $\mathbb{P}_{X,Y}$. We consider a set of L input manipulations, $\mathcal{M} = \{m_1, ..., m_L\}$, and a

manipulation function $q : \mathcal{M} \times \mathcal{X} \to \hat{\mathcal{X}}$ such that $q(m_l, x) = \hat{x}$ applies the manipulation on the input and returns the manipulated output $\hat{x}$. Leaving the input unchanged is represented by the no-op manipulation $m_\varnothing$ with $q(m_\varnothing, x) = x$.

To facilitate evaluation of feature attribution, we require the manipulation effect to be *localized*, in that $q(m, x)$ affects only a part of the input x. Formally, the *effective region* (ER) of m_l on x is the set of input features modified by m_l, denoted as $\phi_l(x) \doteq \left\{ i : [q(m_l, x)]_{(i)} \neq x_{(i)} \right\}$, where subscript (i) indexes over individual features. The ER of the no-op is empty, $\phi_\varnothing = \varnothing$.

From the original distribution $\mathbb{P}_{X,Y}$ (Fig. 1-(1)), the dataset is modified in two steps: label reassignment (Fig. 1-(2)) and input manipulation (Fig. 1-(3) & (4)).

Label Reassignment   Our final goal is to ensure that the model has to rely on certain introduced features (e.g. a watermark) to achieve a high performance. However, the model could in theory use any of the existing features (e.g. medical features) to achieve high accuracy, and thus disregard the new feature, even if it is perfectly correlated with the label. To guarantee the model's usage of input manipulation, we need to weaken the correlation between the original features and the labels.

Specifically, given a reassignment matrix $R \in \mathbb{R}^{K \times K}$, the label reassignment process assigns a new label $\hat{y}$ based on the original label y with probability $R_{y,\hat{y}}$. The expected accuracy $p^{(2)}$ of *any* classifier is now bounded by $p^{(2)} \leq p^* = \max_{i,j} R_{i,j}$. We denote the joint distribution of the input and the reassigned label as $\mathbb{P}_{X,\hat{Y}}$. Note that as an extreme case, if the label is reassigned completely randomly, then the existing features are non-informative to the label, and any performance above the random guess baseline is due to the introduced features.

Input Manipulation   After reassigning labels to bound classifier performance, we apply label-dependent manipulations on the input. For $(x, \hat{y}) \sim \mathbb{P}_{X,\hat{Y}}$, we choose a manipulation m_l from $\mathcal{M}$ and modify the input as $\hat{x} = q(m_l, x)$. The probability of choosing m_l is given by $Q_{\hat{y},l}$ of a manipulation matrix $Q \in \mathbb{R}^{K \times L}$. We denote the data distribution after this step as $\mathbb{P}_{\hat{X},\hat{Y}}$. With appropriate choice of Q and $\mathcal{M}$, $\mathbb{P}_{\hat{X},\hat{Y}}$ can satisfy $\hat{p}^* \doteq \sup_{\hat{x},\hat{y}} \mathbb{P}_{\hat{Y}|\hat{X}}(\hat{y}|\hat{x}) > p^*$. For example, we can achieve $\hat{p}^* = 1$ when a watermark is only applied to one (post-reassignment) class.

Whenever a model trained on $(\hat{\mathcal{X}}, \hat{\mathcal{Y}})$ achieves expected *accuracy $p^{(4)} > p^*$, it is guaranteed to rely on the knowledge of manipulation, which is solely confined within the joint effective region $\phi_\cup(x) \doteq \cup_l \phi_l(x)$.* This gives us a straightforward sanity check for feature attribution methods: they should recognize the contribution inside $\phi_\cup(x)$. For our example, since only the watermark is applied to one class, $\phi_\cup$ is the same as the watermarked region.

On finite test sets, due to stochasticity in label reassignment, a classifier can achieve an accuracy $p > p^*$ without using the manipulation. However, for test set size N, the probability of achieving of p or higher by this classifier, with *expected* accuracy bounded by p^*, is at most $\sum_{n=\lfloor pN \rfloor}^{N} \text{Binom}(n; N, p^*)$, which vanishes quickly with increasing N and p.

Remark. It is crucial that we consider the *joint* ER for attribution values, because a model could use the absence of evidence as a legitimate basis for decision. For example, consider an image dataset, with each image having a watermark either on the top or bottom edge. The positive/negative labels are correlated with top/bottom watermark respectively. A model could predict the negative class by observing the *absence* of a watermark on the top edge. In this case, the correct attribution to the top edge is within the joint ER but *not* within the bottom watermark ER. Current evaluations [2, 31] often omit this possibility by using the ER of only the manipulation corresponding to the target class rather than all possible ones, potentially rejecting correct attributions.

In next three sections, we experimentally compare attribution values computed by three types of models—saliency maps, attention mechanisms, and rationale models—to those expected by the desiderata, identify their deficiencies and give recommendations for improvements.

5   Evaluating Image Saliency Maps

For this set of experiments, we simulate a common scenario where a model seemingly achieves "superhuman" performance on some very hard task, only to later find out that it uses some image artifacts which are accidentally leaked in during the data collection process. We evaluate the extent to which attribution methods can identify such artifacts.

Dataset: We curated our own dataset on bird species identification. It is motivated by CUB-200-2011 [29], with a large number of high-resolution images for fine-grained classification. We identified the four most mistaken class pairs in CUB-200-2011 by a ResNet-34 model [10] and scraped Flickr for 1,200 new images for each of these classes. We center-cropped all image to 224×224 and mean-variance normalized using ImageNet statistics [9]. We split the 1,200 images per class into train/validation/test sets of 1000/100/100 images. Fig. 2 presents sample images, the test set confusion matrix for a ResNet-34 model trained on it, and saliency maps for a correct prediction (Fish Crow).
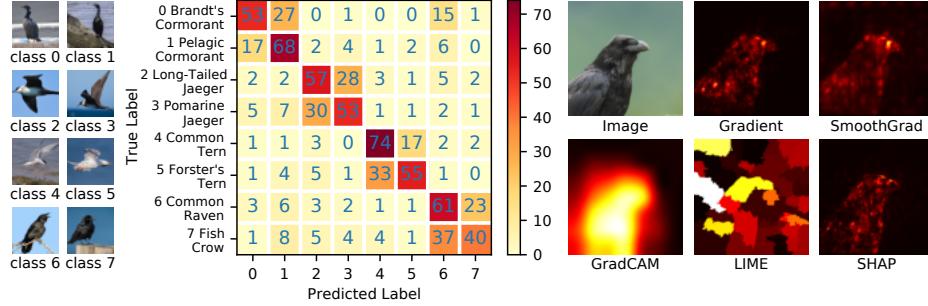

Figure 2: Left: Dataset samples. Middle: Test set confusion matrix of a ResNet-34 model. Right: Examples of five different saliency maps for a correct prediction.

Input Manipulations: We select five representative image manipulations that correspond to artifacts that could be accidentally introduced in a dataset collection process: blurring, brightness change, hue change, pixel noise, and watermark. Details and examples of each manipulation are in App. A.1.

Saliency Maps: We evaluate 5 standard saliency map methods: Gradient [27], SmoothGrad [28], GradCAM [24], LIME [21], and SHAP [17]. These methods are described in detail in App. A.2.

Experiments: We choose pairs of similar species (e.g. common tern and Forester's tern) to simulate a hard task which is accidentally made easier through the presence of artifacts. All experiments are binary classifications. Sec. 5.4 also uses pairs of distinct species (e.g. common tern and fish crow).

Metric: We study the attribution percentage assigned to the joint effective region $\mathrm{Attr}\%(\phi_\cup)$. We calculate $\%\mathrm{Attr}$ for images in the test set, and report the average separately for the two classes.

In label reassignment, the label is preserved with probability r, and flipped otherwise. It is obvious that the accuracy without relying on the manipulation is at most $\max(r, 1-r)$. A manipulation is applied to the positive class and $m_\varnothing$ is applied to the negative class (i.e. leaving it unchanged).

5.1 Attribution vs. Effective Region Size

Question: How well do saliency maps give attribution to the manipulations for (near-)perfect models?

Setup: We trained 100 models, each on a randomly selected pair of similar species and a randomly selected manipulation type. We reassign labels with $r = 0.5$, and apply the manipulation to images of the positive post-reassignment class, leaving those of the negative class unchanged.

Expectation: Due to $r = 0.5$, only the manipulation is correlated with the label. A near-perfect performance thus indicates that the model strongly relies on features inside $\phi_\cup$ and is barely distracted by features outside of it. Thus, we should expect $\mathrm{Attr}\%(F_{\phi_\cup}) \approx 1.0$, regardless of the size of $\phi_\cup$.

Results: Around 70% of all runs achieve test accuracy of over 95%, and we compute $\mathrm{Attr}\%(F_{\phi_\cup})$ for these models only and plot them against $\%\mathrm{ER}$, defined as the size of $\phi_\cup$ as a fraction of total image size. Fig. 3 shows these two values for some methods and manipulations. The complete result is shown in Fig. 13 of App. A.3. Blue/orange markers are for the positive/negative classes with/without the manipulation applied. The green horizontal line plots $\mathrm{Attr}\%(F_{\phi_\cup}) \approx 1.0$ and the red diagonal line indicates the behavior of a random saliency map.

None of the methods consistently scores $\%\mathrm{Attr} \approx 1$ on all manipulations. SHAP performs the best, achieving $\%\mathrm{Attr} = 69\%$ at $\%\mathrm{ER} = 40\%$ on average. However, its success varies widely across manipulation types: on watermark it achieves $\%\mathrm{Attr} = 82\%$ at $\%\mathrm{ER} = 31\%$ while on blurring it only scores $\%\mathrm{Attr} = 47\%$ at $\%\mathrm{ER} = 36\%$. LIME performs the worst ($\%\mathrm{Attr} = 49\%$ on average), most likely because the image segmentation fails to isolate the manipulated features.
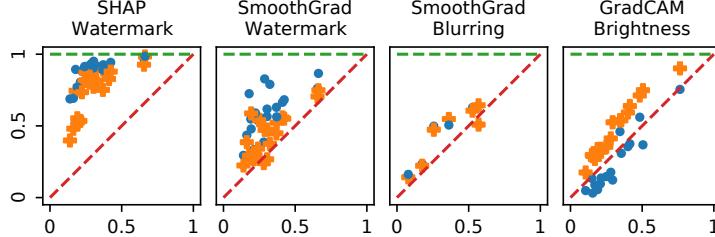
Figure 3: %Attr (y-axis) vs. %ER (x-axis). Blue circles and orange crosses are for images with and without the manipulation. Green horizontal line indicates the ideal saliency map and red diagonal line indicates a random saliency map. Complete results are in Fig. 13 of App. A.3.

Similar inconsistency applies to manipulation types too. Watermark is the most successfully detected by all methods, with %Attr $= 56\%$ at %ER $= 31\%$, possibly due to its "object-like" property which is found to be implicitly learned by convolutional layers [7], and blurring the least, with %Attr $= 45\%$ at %ER $= 36\%$, for the lack of it.

In addition, the presence of manipulations is more easily detected than the absence (%Attr $= 59\%$ vs 56%), likely because the model works by implicitly localizing objects [7] and predicting a default negative class if it fails. It is also much easier for perturbation-based methods such as LIME to "hide" the manipulation when it is present than to "construct" it when absent. This may mislead people about the true reason for a negative prediction, and better methods to convey the absence are desirable.

5.2 Attribution vs. Test Accuracy

Question: How does %Attr change as the model's test accuracy increases during training?

Setup: We use the the same setup as Sec. 5.1.

Expectation: As the test accuracy increases, the model must rely more and more on knowledge of manipulation. As a result, we should expect $\text{Attr}\%(F_{\phi_\cup})$ to also increase.

Results: For the training run of each model, we compute $\text{Attr}\%(F_{\phi_\cup})$ not only for the best model, but also for models during the intermediate epochs with various test accuracy. Fig. 4 plots the lines representing the progress of %Attr vs. test accuracy, with complete result shown in Fig. 16 of App. A.6. SHAP on watermark show the most consistent increase in %Attr with test accuracy. For other saliency maps and feature types, the trend is either very mild or very noisy.
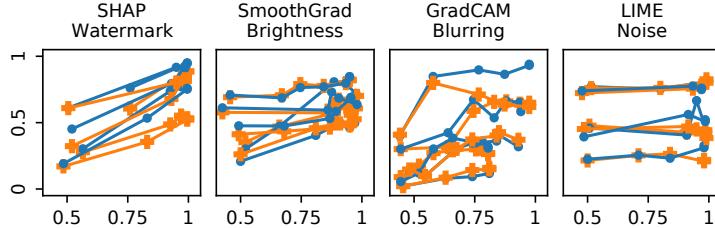

Figure 4: %Attr (y-axis) vs. test accuracy (x-axis). Blue/orange colors indicate manipulation presence/absence. Complete results are in Fig. 16 of App. A.6.

5.3 Attribution vs. Manipulation Visibility

Question: How well can the saliency map recognize manipulations of different visibility levels?

Setup: We conduct 100 runs, with 20 per manipulation. We further group the 20 runs into 4 groups, with 5 runs in a group using the same manipulation type and effective region but varying degrees of visibility, detailed in App. A.4. For example, the visibility for a watermark refers to its font size. As before, the labels are reassigned with $r = 0.5$ and manipulations applied to the positive class.

Expectation: A good saliency map should not be affected by manipulation visibility, as long as the model is objectively using it. However, different saliency maps may be better suited to detect more or less visible manipulations. For example, a less visible manipulation may be ignored by the segmentation algorithm used by LIME, while inducing larger gradients in the decision space.

6

Results: Fig. 5 plots each group of five runs as a line, with visibility level on the x-axis and %Attr on the y-axis. The complete result is shown in Fig. 14 of App. A.4. We discovered a wide variety of behaviors. As the manipulation becomes more visible, SHAP generally assign higher attribution values, LIME and GradCAM attributions stays roughly constant, and gradient attributions diverge depending on whether manipulations are present or absent.
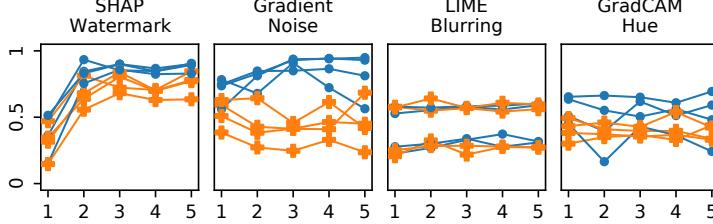

Figure 5: %Attr (y-axis) vs. feature visibility (x-axis). Blue and orange colors indicate feature presence or absence. Complete results are in Fig. 14 of App. A.4.

5.4 Attribution vs. Original Feature Correlation

Question: How does the attribution on the manipulation change if the label reassignment is correlated with the original input features to varying degrees (i.e. $r \in [0.5, 1.0]$)?

Setup: For each manipulation, we vary the label reassignment parameter $r \in \{0.5, 0.6, 0.7, 0.8, 0.9, 1.0\}$. For each r, we train four models on four class pairs, two of similar species and two of distinct ones (e.g. fish crow and common tern). These variations total $5 \times 6 \times 4 = 120$ runs.

Expectation: For $r > 0.5$, there is no standard definition of the attribution value on the original image features and the manipulations, as any decreasing trend of %Attr with increasing r is reasonable. However, the Shapley value [22] is a commonly used axiomatic definition for feature attributions. We denote the set of features inside the effective region as F_M, for manipulated features, and that outside as F_O, for original features. Their Shapley values on performance $v(F_M)$ and $v(F_O)$ are defined as

$$v(F_M) = \tfrac{1}{2}\left[a(F_M) - a(\varnothing) + a(F_M \cup F_O) - a(F_O)\right], \tag{1}$$

$$v(F_O) = \tfrac{1}{2}\left[a(F_O) - a(\varnothing) + a(F_M \cup F_O) - a(F_M)\right], \tag{2}$$

where $a(F_M), a(F_O), a(\varnothing)$, and $a(F_M \cup F_O)$ refers to the classifier's expected accuracy when only F_M, only F_O, neither, and both are available, respectively. For a classifier with accuracy p, we have $a(\varnothing) = 0.5$, $a(F_M) = a(F_M \cup F_O) = p$, and $a(F_O) \leq r$. The formal definition of $a(\cdot)$ and its calculation are in App. A.5. We normalize the Shapley values to $\bar{v}(F_M)$ and $\bar{v}(F_O)$ by their sum $\bar{v}(F_M) + \bar{v}(F_O)$. It is easy to see that

$$\bar{v}(F_M) \geq (2p - r - 0.5)/(2p - 1), \tag{3}$$

$$\bar{v}(F_O) \leq (r - 0.5)/(2p - 1). \tag{4}$$

For (near-)perfect classifier with $p \approx 1$, we have $\bar{v}(F_M) \geq 1.5 - r$, and $\bar{v}(F_O) \leq r - 0.5$. In addition, $a(F_O)$ should be close to r for the distinct pair as the model can better utilize the more distinct original image features, resulting in lower attribution $\bar{v}(F_M)$ on manipulated features.

Results: All models achieve test accuracy of over 95%. Fig. 6 plots %Attr vs. r. The complete result is shown in Fig. 15 of App. A.5. Solid lines represent runs with a similar species pair, and dashed lines represent runs with a distinct species pair. The green shaded area represents the area of $\bar{v}(F_M) \geq 1.5 - r$, the Shapley value range at $p = 1$. Intuitively, for r close to 0.5, the correlation between F_O and the label are very weak, and the theoretical Shapley values should mostly concentrate on F_M for the (near-)perfect model, with %Attr close to 1. As r increases to 1, the model can choose to rely more heavily on F_O for its prediction, resulting in larger allowable ranges of %Attr.

For watermark feature injection, SHAP shows clear decreases in attribution value as r increases, while gradient also tracks the predicted range, but only for the class with the manipulation. This trend is not seen in other feature types, which shows relative insensitivity with respect to r. In addition, there does not seem to be a clear difference in attribution values for similar vs. distinct species pairs.

5.5 Discussion

The set of experiments simulates the setting in which a model uses unexpected artifacts to achieve high performance, and none of the saliency maps could consistently detect such usage in various
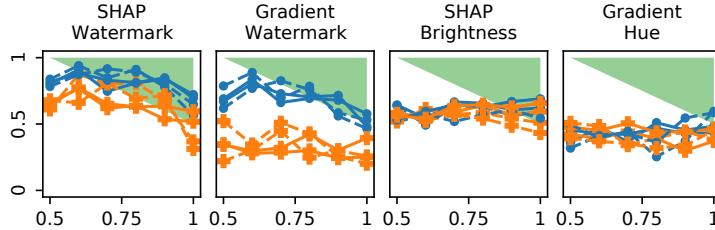
Figure 6: $\%\mathrm{Attr}$ (y-axis) vs. r (x-axis). Blue/orange colors indicate feature presence/absence. Solid/dashed lines represent the results for similar/distinct species pairs. The green shade represents $\bar{v}(F_M) \geq 1.5 - r$, i.e. Shapley value range at $p = 1$. Complete results are in Fig. 15 of App. A.5.

settings such as model performance and artifact visibility, casting doubts on their effectiveness for real-world datasets and models, such as the opening example in Sec. 1.

6 Evaluating Text Attentions

It is known that certain non-semantic features can heavily influence model prediction [21]. We study whether the word attention score can saliently highlight any potential usage of such non-semantic features. Details of the implemented dot-product attention mechanism are presented in App. B.1.

Dataset: We use the review text of the BeerAdvocate dataset [18] as the input and the appearance score as the target. For unknown reasons, there is a significant mismatch between the training and test sets: only 9% of training reviews have a score of 8 while 46% of test reviews do. To ensure a controlled setting, we select from the training set 6,000 reviews with score of 5 and 6 each, as the negative and positive classes, and create our own splits of 10,000/1,000/1,000 reviews.

Metric: The introduced manipulation changes specific words according to the (reassigned) label. The metric is $\%\mathrm{Attr}$ defined on the set of target words (i.e. effective region).

6.1 Highly Obvious Correlating Features

Question: How well can attention scores focus on highly obvious manipulations?

Setup: From our filtered dataset, we first reassign labels with $r = 0.5$. For the positive reviews, we change all the article words (*a / an / the*) to "the", and for the negative reviews, we change these to "a". Thus, the articles are the only words correlated with the labels and constitute the effective region.

Expectation: Attentions of (near-)perfect models should have $\%\mathrm{Attr} \approx 1$ to be valid attributions.

Results: The model achieves over 97% accuracy. Across the test set, $\%\mathrm{Attr}$ on article words is 8.6%. Considering that articles are 7.9% of all words, this is better than random, albeit barely. Fig. 7 visualizes the attention distribution for two reviews, with additional results in Fig. 17 of App. B.2. Each bars represent weights of words in the review. Green bars represent non-articles and orange bars represent articles. In some cases article attentions do not stand out from the rest. In other cases, they stand out only *relative* to their neighbors.
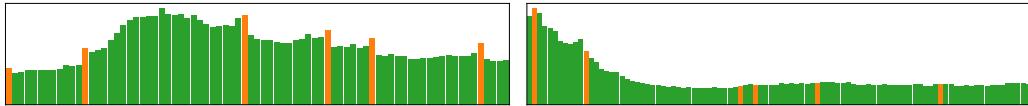

Figure 7: Attention values for each token in two reviews. Orange/green bars represent articles/non-articles. More in Fig. 17 of App. B.2.

6.2 Misleading Non-Correlating Features

Question: When some features are known to not correlate with the label but are very similar to correlating ones, do attention scores also focus on these non-correlating ones?

Setup: Again from our filtered dataset, we applied two similar manipulations, with only one of them is correlated with the (reassigned) label. Fig. 8 details the construction of two datasets, *CN* and *NC*.

Expectation: Same as above. In particular, non-correlating articles should *not* be attended to.
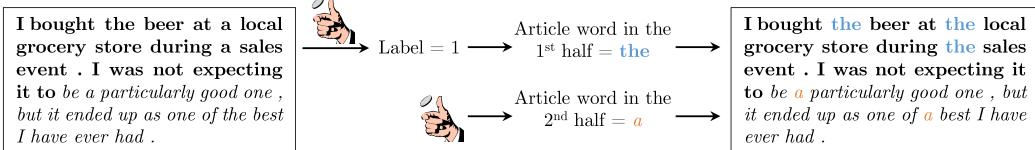
8

I bought the beer at a local grocery store during a sales event . I was not expecting it to *be a particularly good one , but it ended up as one of the best I have ever had .*

Label = 1 ⟶ Article word in the 1st half = the ⟶

Article word in the 2nd half = a ⟶

I bought the beer at the local grocery store during the sales event . I was not expecting it to *be a particularly good one , but it ended up as one of a best I have ever had .*

Figure 8: The process to build *CN* dataset for the experiment in Sec. 7.2. First, a review is split into two halves at the midpoint, shown in **bold** and *italics*. Then a label is randomly sampled and assigned to the review. Depending on the label, the articles in the first half are changed to "a" or "the". They are called *correlating articles*. Then an article word is randomly chosen for the second half, and all articles in the second half are changed to that word. They are called *non-correlating articles*. For *NC* dataset, the roles of two halves are switched.

Results: The models on both datasets achieve over 97% accuracy. Fig. 9 presents attention visualization, with more in Fig. 18 of App. B.3. The two models show very different behaviors. The *CN* model exclusively focuses attentions on correlating articles, while the *NC* model behaves similarly to the previous experiment. Unlike the rationale models, however, the *NC* model does not assign any higher weights to non-correlating articles.
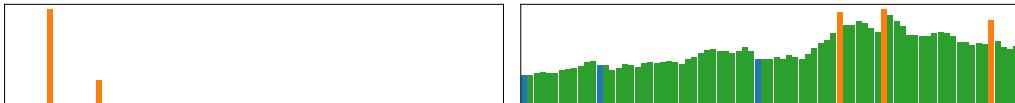
Figure 9: Attention scores for one review in *CN* (left) and *NC* (right) dataset. Orange/blue/green bars represent corr. articles/non-corr. articles/other words. More in Fig. 18 of App. B.3.

Observing the large variation of behaviors, we further trained the three models ten more times to see if any consistent attention pattern exists. All models achieve over 97% accuracy. Tab. 1 presents the mean and standard deviation statistics for the 11 runs. The clean attention pattern by the *CN* model does not persist, and the model sometimes assigns higher than random weights on non-correlating articles, especially for the NC dataset. These results further suggests that attention weights cannot be readily and reliably interpreted as attributions without further validation.

Dataset	Corr. Articles	Non-Corr. Articles	Other Words
Article	$(10.3\% \pm 2.4\%)/7.9\%$	NA	$(89.7\% \pm 2.4\%)/92.1\%$
CN	$(15.9\% \pm 25.7\%)/4.1\%$	$(5.9\% \pm 4.0\%)/3.8\%$	$(78.2\% \pm 24.7\%)/92.1\%$
NC	$(12.0\% \pm 8.4\%)/3.8\%$	$(12.6\% \pm 9.3\%)/4.1\%$	$(75.4\% \pm 16.7\%)/92.1\%$

Table 1: Attention attribution statistics over 11 training runs, in the format of $(\text{mean}(\%\text{Attr}) \pm \text{stdev}(\%\text{Attr}))/$word frequency. The "Article" dataset is the one used in Sec. 6.1.

6.3 Discussion

Attention mechanism is undoubtedly useful, but its *interpretation* as attribution is under debate. On our studies, the answer is mostly negative: for most training runs, the attention weights on correlating features at best only stand out *locally*, easily overwhelmed by larger global variations. Past studies proposed various, and sometimes conflicting, criteria for attentions to be considered as attribution explanation [13, 30]. However, it is not clear whether they correspond to any ground truth attribution, and we recommend future proposals to first be calibrated with ground truth in a controlled setting.

While our manipulations introduce artifacts such as misused articles, similar artifacts have been identified to affect model prediction. For example, an SVM classifier uses the text header information [21] on the 20 Newsgroups task [15], and it is crucial for attribution methods to detect it.

7 Evaluating Text Rationales

In this section, we conducted the same two experiments above (and omit the **Question** and **Setup** descriptions), but for two rationale models, a reinforcement learning (RL) model [16] and a continuous relaxation (CR) model [6]. In the original forms, both models regularize the rationale length and continuity. In our experiments, rather than regularizing the length, we train the models to produce

rationales that match a target selection rate $\%$Sel. For a mini-batch of B examples, we use

$$\lambda \cdot \left| \sum_{i=1}^{B} \text{len}(\text{rationale}_i) / \sum_{i=1}^{B} \text{len}(\text{review}_i) - \text{Sel}\% \right|, \tag{5}$$

where $\lambda > 0$ is the regularization strength. Incidentally, we also found that the training is much more stable with this regularization, especially for the RL model. Additionally, we removed the discontinuity penalty, because the ground truth rationales in our experiments are not continuous.

Metric: As discussed in Sec. 3, we use the precision and recall metrics.

7.1 Highly Obvious Manipulations

Expectation: A necessary condition for a non-misleading rationale is that it should include at least one article word, regardless of selection rate. However, a desirable property of rationale is comprehensiveness [32]: selecting as many article words as possible. Thus, a good rationale model should have high precision when selection rate is low and high recall when selection rate is high.

Results: We trained models with $\%$Sel $\in \{0.07, 0.09, 0.11, 0.13, 0.15\}$, all with over 97% accuracy. We evaluate precision and recall of the trained models and plot them in Fig. 10 (left) according to the actual rationale selection rate, $\%$Sel, on the test set. Blue and orange markers are for the RL and CR models respectively. The two green lines show two optimality notions: the solid line enforces aggregate $\%$Sel for the test set, and the dashed line enforces $\%$Sel individually per review.
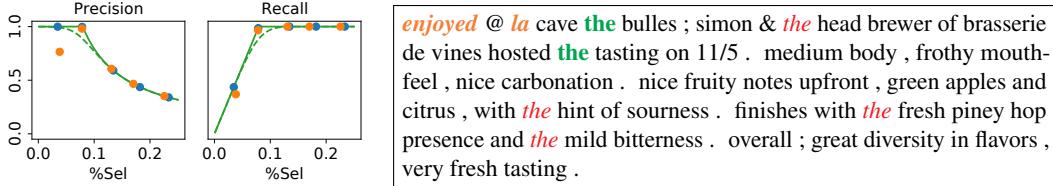

Figure 10: Left: Precision and recall for two rationale models, RL in blue and CR in orange. The solid and dashed green lines show optimal metric values when $\%$Sel is enforced at dataset- and sentence-level. Right: Sample rationales extracted by the CR model at lowest $\%$Sel: selected non-articles in *orange bold italics*, selected articles in **green bold**, and missed articles in *red italics*. Additional examples are in Fig. 19 of App. C.1.

Except for the CR model at the lowest $\%$Sel, all other models achieve near-perfect rationale selection on both the precision and and the recall metrics. The metric values track the dataset-wide optimal values, because selection rate regularization is done at the mini-batch level in Eq. 5. The "faulty" CR model has a tendency of selecting the first couple words regardless, as shown in Fig. 10 (right). However, it still successfully selects some article words.

7.2 Misleading Non-Correlating Features

Expectation: Similar to the previous experiment, the desiderata only require at least one correlating article word to be selected. However, selection of non-correlating articles is arguably more misleading than selection of other non-article words, because it suggests that these non-correlating articles also influence the prediction, even though the classifier simply learns to ignore them.

Results: We trained models with $\%$Sel $\in \{0.03, 0.05, 0.07, 0.09\}$, all with over 97% accuracy. Fig. 11 (top) plots the precision of correlating articles for the two datasets, as well as the dataset-wide optimal value. We found the rationales consist of almost exclusively article words (Fig. 11 right). However, especially for the RL model, some correlating articles are missed while at the same time non-correlating ones are selected, resulting in less than optimal precision.

7.3 Discussion

Both rationale models produce rationales that include some ground truth correlated feature, showing that the selector can identify important features for the classifier. However, we also observed selection of misleading non-correlating features *even at low selection rates*, potentially obfuscating the model's reasoning process by giving *more* but unnecessary information to the human. It seems to be consistently more severe with RL training, possibly due to the difficulty with the REINFORCE optimization. Future work may be needed to further prune rationales in some way.
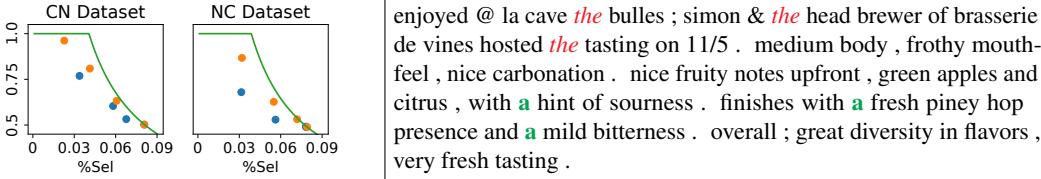
enjoyed @ la cave *the* bulles ; simon & *the* head brewer of brasserie de vines hosted *the* tasting on 11/5 . medium body , frothy mouth-feel , nice carbonation . nice fruity notes upfront , green apples and citrus , with **a** hint of sourness . finishes with **a** fresh piney hop presence and **a** mild bitterness . overall ; great diversity in flavors , very fresh tasting .

Figure 11: Left: Precision at different %Sel for the two datasets. Right: One review of *NC* dataset with rationales highlighted, correlating in **green bold** and non-correlating in *red italics* (no non-article words are selected). Additional examples are in Fig. 20 of App. C.2.

8 Conclusion

It is important for feature attribution methods to faithfully reflect the model's reasoning process, but evaluation is hard without the ground truth knowledge. In this paper, we proposed a dataset modification procedure such that *any* model achieving a sufficiently high performance has to rely on a set of known and well-defined features. This guarantee opens up avenues for automatic evaluation of attribution methods in a principled manner. In our experiments, we evaluate saliency maps, rationale models, and attention mechanisms on vision and language tasks, and identify their deficiencies.

A limitation of our evaluation is that the use of semi-natural datasets in which input manipulation tends to create artifacts, and the identified problems may be less severe on natural datasets. Nonetheless, the modification process does represent realistic dataset corruptions such as presence/absence of watermark in images from different sources. Furthermore, any limitations of attribution methods should be carefully studied, and practitioners should be accordingly informed of them.

References

[1] Julius Adebayo, Justin Gilmer, Michael Muelly, Ian Goodfellow, Moritz Hardt, and Been Kim. Sanity checks for saliency maps. In *Advances in neural information processing systems*, volume 31, pages 9505–9515, 2018.

[2] Julius Adebayo, Michael Muelly, Ilaria Liccardi, and Been Kim. Debugging tests for model explanations. *arXiv preprint arXiv:2011.05429*, 2020.

[3] Leila Arras, Ahmed Osman, Klaus-Robert Müller, and Wojciech Samek. Evaluating recurrent neural network explanations. In *Proceedings of the 2019 ACL Workshop BlackboxNLP: Analyzing and Interpreting Neural Networks for NLP*, pages 113–126, 2019.

[4] Sebastian Bach, Alexander Binder, Grégoire Montavon, Frederick Klauschen, Klaus-Robert Müller, and Wojciech Samek. On pixel-wise explanations for non-linear classifier decisions by layer-wise relevance propagation. *PloS one*, 10(7):e0130140, 2015.

[5] Dzmitry Bahdanau, Kyunghyun Cho, and Yoshua Bengio. Neural machine translation by jointly learning to align and translate. *arXiv preprint arXiv:1409.0473*, 2014.

[6] Jasmijn Bastings, Wilker Aziz, and Ivan Titov. Interpretable neural predictions with differentiable binary variables. In *Proceedings of the 57th Annual Meeting of the Association for Computational Linguistics*, pages 2963–2977, 2019.

[7] David Bau, Bolei Zhou, Aditya Khosla, Aude Oliva, and Antonio Torralba. Network dissection: Quantifying interpretability of deep visual representations. In *Proceedings of the IEEE conference on computer vision and pattern recognition*, pages 6541–6549, 2017.

[8] Ian Covert, Scott Lundberg, and Su-In Lee. Understanding global feature contributions through additive importance measures. *arXiv preprint arXiv:2004.00668*, 2020.

[9] Jia Deng, Wei Dong, Richard Socher, Li-Jia Li, Kai Li, and Li Fei-Fei. Imagenet: A large-scale hierarchical image database. In *2009 IEEE conference on computer vision and pattern recognition*, pages 248–255. Ieee, 2009.

[10] Kaiming He, Xiangyu Zhang, Shaoqing Ren, and Jian Sun. Deep residual learning for image recognition. In *Proceedings of the IEEE conference on computer vision and pattern recognition*, pages 770–778, 2016.

[11] Sara Hooker, Dumitru Erhan, Pieter-Jan Kindermans, and Been Kim. A benchmark for interpretability methods in deep neural networks. *arXiv preprint arXiv:1806.10758*, 2018.

[12] Aya Abdelsalam Ismail, Mohamed Gunady, Héctor Corrada Bravo, and Soheil Feizi. Benchmarking deep learning interpretability in time series predictions. *arXiv preprint arXiv:2010.13924*, 2020.

[13] Sarthak Jain and Byron C Wallace. Attention is not explanation. *arXiv preprint arXiv:1902.10186*, 2019.

[14] Sarthak Jain, Sarah Wiegreffe, Yuval Pinter, and Byron C Wallace. Learning to faithfully rationalize by construction. *arXiv preprint arXiv:2005.00115*, 2020.

[15] Ken Lang. Newsweeder: Learning to filter netnews. In *Machine Learning Proceedings 1995*, pages 331–339. Elsevier, 1995.

[16] Tao Lei, Regina Barzilay, and Tommi Jaakkola. Rationalizing neural predictions. In *Proceedings of the 2016 Conference on Empirical Methods in Natural Language Processing*, pages 107–117, 2016.

[17] Scott Lundberg and Su-In Lee. A unified approach to interpreting model predictions. *arXiv preprint arXiv:1705.07874*, 2017.

[18] Julian McAuley, Jure Leskovec, and Dan Jurafsky. Learning attitudes and attributes from multi-aspect reviews. In *2012 IEEE 12th International Conference on Data Mining*, pages 1020–1025. IEEE, 2012.

[19] Milad Mostavi, Yu-Chiao Chiu, Yufei Huang, and Yidong Chen. Convolutional neural network models for cancer type prediction based on gene expression. *BMC medical genomics*, 13:1–13, 2020.

[20] Danish Pruthi, Mansi Gupta, Bhuwan Dhingra, Graham Neubig, and Zachary C Lipton. Learning to deceive with attention-based explanations. In *Proceedings of the 58th Annual Meeting of the Association for Computational Linguistics*, pages 4782–4793, 2020.

[21] Marco Tulio Ribeiro, Sameer Singh, and Carlos Guestrin. "Why should I trust you?" Explaining the predictions of any classifier. In *Proceedings of the 22nd ACM SIGKDD international conference on knowledge discovery and data mining*, pages 1135–1144, 2016.

[22] Alvin E Roth. *The Shapley value: essays in honor of Lloyd S. Shapley*. Cambridge University Press, 1988.

[23] W. Samek, A. Binder, G. Montavon, S. Lapuschkin, and K. Müller. Evaluating the visualization of what a deep neural network has learned. *IEEE Transactions on Neural Networks and Learning Systems*, 28(11):2660–2673, 2017. doi: 10.1109/TNNLS.2016.2599820.

[24] Ramprasaath R Selvaraju, Michael Cogswell, Abhishek Das, Ramakrishna Vedantam, Devi Parikh, and Dhruv Batra. Grad-cam: Visual explanations from deep networks via gradient-based localization. In *Proceedings of the IEEE international conference on computer vision*, pages 618–626, 2017.

[25] Li Shen, Laurie R Margolies, Joseph H Rothstein, Eugene Fluder, Russell McBride, and Weiva Sieh. Deep learning to improve breast cancer detection on screening mammography. *Scientific reports*, 9(1):1–12, 2019.

[26] Ke Si, Ying Xue, Xiazhen Yu, Xinpei Zhu, Qinghai Li, Wei Gong, Tingbo Liang, and Shumin Duan. Fully end-to-end deep-learning-based diagnosis of pancreatic tumors. *Theranostics*, 11 (4):1982, 2021.

[27] Karen Simonyan, Andrea Vedaldi, and Andrew Zisserman. Deep inside convolutional networks: Visualising image classification models and saliency maps. *arXiv preprint arXiv:1312.6034*, 2013.

[28] Daniel Smilkov, Nikhil Thorat, Been Kim, Fernanda Viégas, and Martin Wattenberg. Smoothgrad: removing noise by adding noise. *arXiv preprint arXiv:1706.03825*, 2017.

[29] C. Wah, S. Branson, P. Welinder, P. Perona, and S. Belongie. The Caltech-UCSD Birds-200-2011 Dataset. Technical Report CNS-TR-2011-001, California Institute of Technology, 2011.

[30] Sarah Wiegreffe and Yuval Pinter. Attention is not not explanation. *arXiv preprint arXiv:1908.04626*, 2019.

[31] Mengjiao Yang and Been Kim. Benchmarking attribution methods with relative feature importance. *arXiv preprint arXiv:1907.09701*, 2019.

[32] Mo Yu, Shiyu Chang, Yang Zhang, and Tommi Jaakkola. Rethinking cooperative rationalization: Introspective extraction and complement control. In *Proceedings of the 2019 Conference on Empirical Methods in Natural Language Processing and the 9th International Joint Conference on Natural Language Processing (EMNLP-IJCNLP)*, pages 4085–4094, 2019.

[33] Bolei Zhou, Aditya Khosla, Agata Lapedriza, Aude Oliva, and Antonio Torralba. Learning deep features for discriminative localization. In *Proceedings of the IEEE conference on computer vision and pattern recognition*, pages 2921–2929, 2016.

A   Additional Details and Results for Saliency Map Evaluations

A.1   Manipulation Types

We consider five image manipulation types. These manipulations are designed to simulate possible image artifacts, which an undesirable model may rely on to make decisions. Each manipulation has parameters which define the effective region and the visibility level of the manipulation effect. Some of the manipulation effects are technically stochastic, such as a watermark being placed in a random position, but the effective region captures the localized manipulation effect of all possible random instantiations. The five manipulations are described below, with examples of each manipulation and their associated effective regions shown in Fig. 12.

- **Peripheral blurring** applies a Gaussian filter to the part of the image outside of a certain radius. It is parametrized by
    - the radius of the *unaffected* part; and
    - the standard deviation of the Gaussian blurring filter.

- **Central brightness shift** gradually changes the brightness in the hue-saturation-brightness (HSB) space inside a certain radius, with maximal change in the center. For our experiments, the brightness change is negative, meaning that the center is dimmed. It is parametrized by
    - the radius of the dimmed region; and
    - the magnitude of the brightness shift at the center.

- **Striped hue shift** modifies the hue (i.e. color) value of a vertical stripe in the image. From top to bottom in the stripe, the hue value is first increased and then decreased in a sinusoidal pattern. It is parametrized by
    - the upper position of the stripe;
    - the lower position of the stripe, with the width of the stripe being (upper - lower);
    - the magnitude of sinusoidal pattern.

- **Striped noise** randomly changes pixels inside a vertical stripe to a uniformly random RGB value. It is parametrized by
    - the upper position of the stripe;
    - the lower position of the stripe, with the width of the stripe being (upper - lower);
    - the probability that each pixel is replaced.

- **Watermark** overlays a text reading "IMGxxxx", where "xxxx" are four random digits, to a random location inside a rectangular region. "IMG" is written in white and the digits are written in black. It is parametrized by
    - the upper-left coordinate of the rectangular region;
    - the lower-right coordinate of the rectangular region;
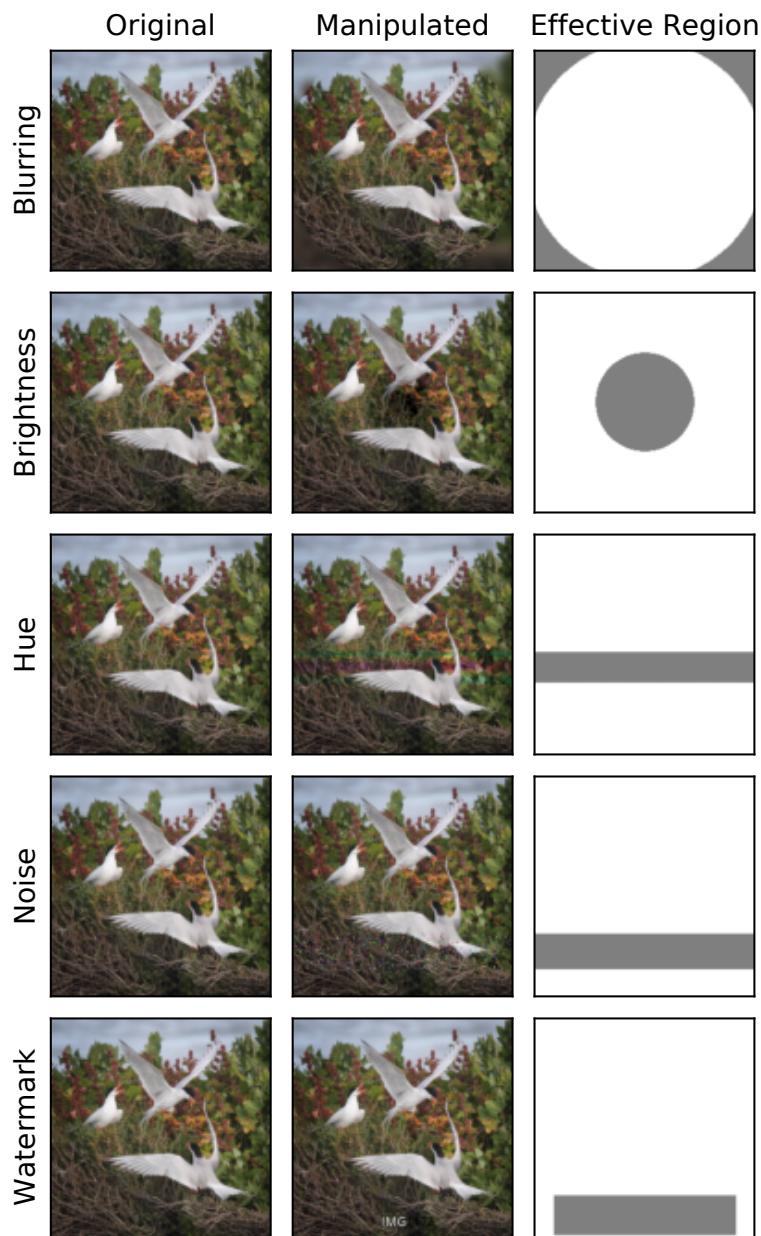   - the font size of the watermark text.

Figure 12: Examples of the five manipulations applied to an image, along with the respective effective regions (ER) shown in gray.

A.2 Saliency Map Methods

We consider five saliency map methods.

- **Gradient** [27] computes the gradient of the logit for the predicted class with respect to the input image. The three channels of gradient are summed up in absolute value to get a single channel.

- **SmoothGrad** [28] averages the gradients on 50 copies of the input image I, each injected with independent Gaussian noise with with $\mu = 0$ and $\sigma = 0.15 \cdot (\max I - \min I)$, where $\max I$ and $\min I$ are the maximal and minimal pixel values of the image.

- **GradCAM** [24] computes a saliency map from convolution filter responses. Since we use the fully convolutional ResNet-34, this method reduces to the class activation mapping (CAM) [33].

- **LIME** [21] performs a linear regression using super-pixels of the input image. The absolute values of the coefficients are used to derive the saliency map. We use the default implementation of `lime.lime_ image.LimeImageExplainer` with the quickshift clustering as the super-pixel segmentation algorithm.

- **SHAP** [17] uses the idea of Shapley value [22] for attribution. We use the GradientSHAP instantiation with the default setting of `shap.GradientExplainer`. We us the entire test set of 200 examples as the "background" data.

A.3 Attribution vs. Effective Region Size

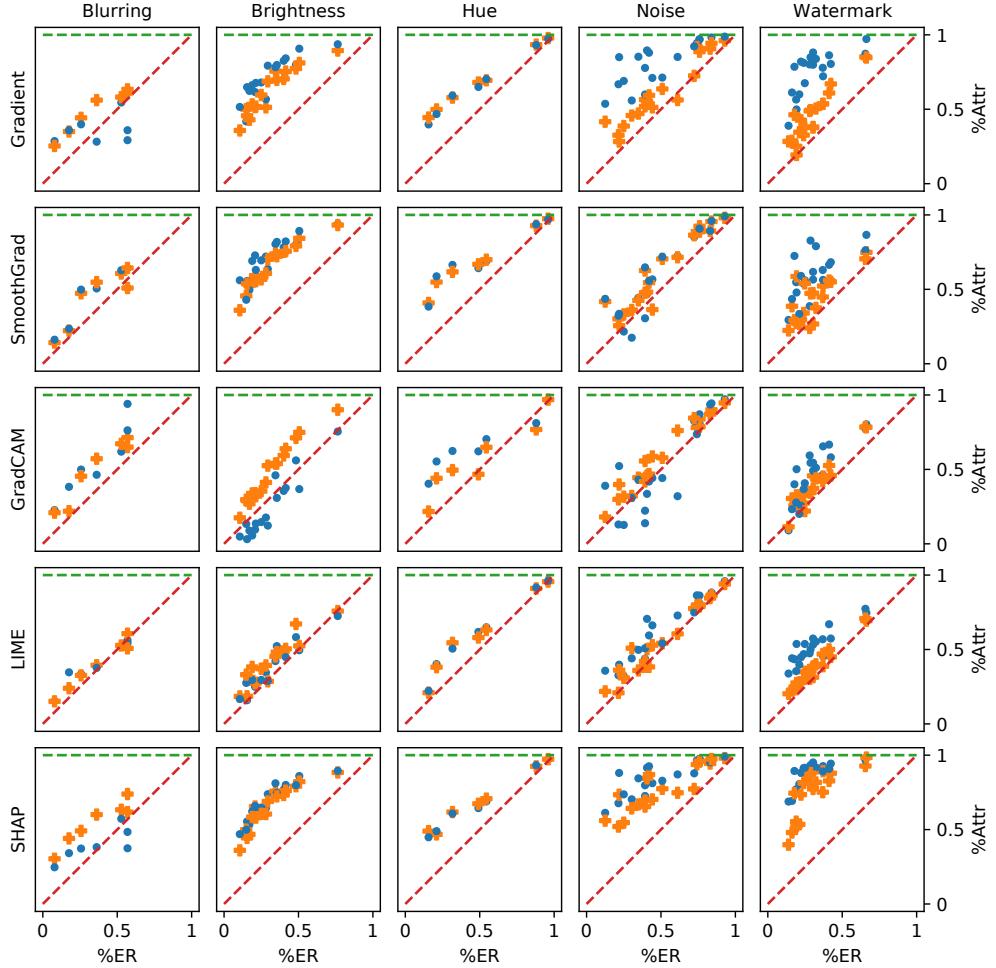Fig. 13 shows %Attr vs %ER for all pairs of saliency maps and manipulations.

Figure 13: %Attr vs %ER for all pairs of saliency maps and manipulations.

A.4 Attribution vs. Manipulation Visibility

Fig. 14 shows $\%\mathrm{Attr}$ vs manipulation visibility for all pairs of saliency maps and manipulations.

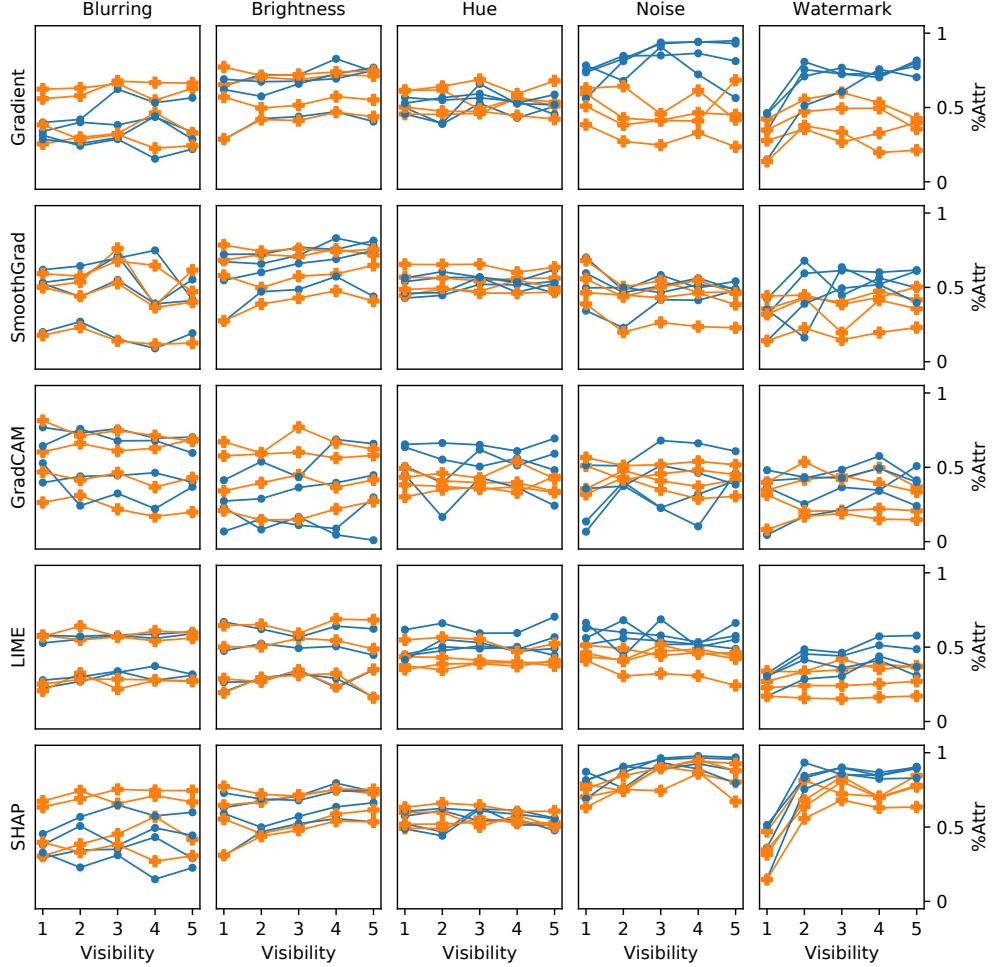Figure 14: $\%\mathrm{Attr}$ vs manipulation visibility for all pairs of saliency maps and manipulations.

We define the five visibility levels for each manipulation type as below. Note that for fair comparison of $\%\mathrm{Attr}$ at different visibility levels, it is crucial that the effective regions are independent of the visibility, which is satisfied in all manipulation types below.

- **Blurring:** The visibility level is defined as the Gaussian blur standard deviation, with values of $\{2, 4, 6, 8, 10\}$ pixels, from least visible to most.

- **Brightness:** The visibility level is defined as the magnitude of the brightness shift, with values of $\{0.1, 0.15, 0.2, 0.25, 0.3\}$ brightness component of the color (in the range of [0, 1]), from least visible to most.

- **Hue:** The visibility is defined as the magnitude of the hue shift, with values of $\{0.05, 0.1, 0.15, 0.2, 0.25\}$ hue component of the color (in the range of [0, 1]), from least visible to most.

- **Noise:** The visibility is defined as the probability that a pixel is replaced by a random value, with values of $\{0.02, 0.04, 0.06, 0.08, 0.1\}$, from least visible to most.

- **Watermark:** The visibility is defined as the font size of the watermark, with values of $\{7, 9, 11, 13, 15\}$ pixels, from least visible to most.

A.5 Attribution vs. Original Feature Correlation

Fig. 15 shows $\%\mathrm{Attr}$ vs the label reassignment parameter r for all pairs of saliency maps and manipulations.
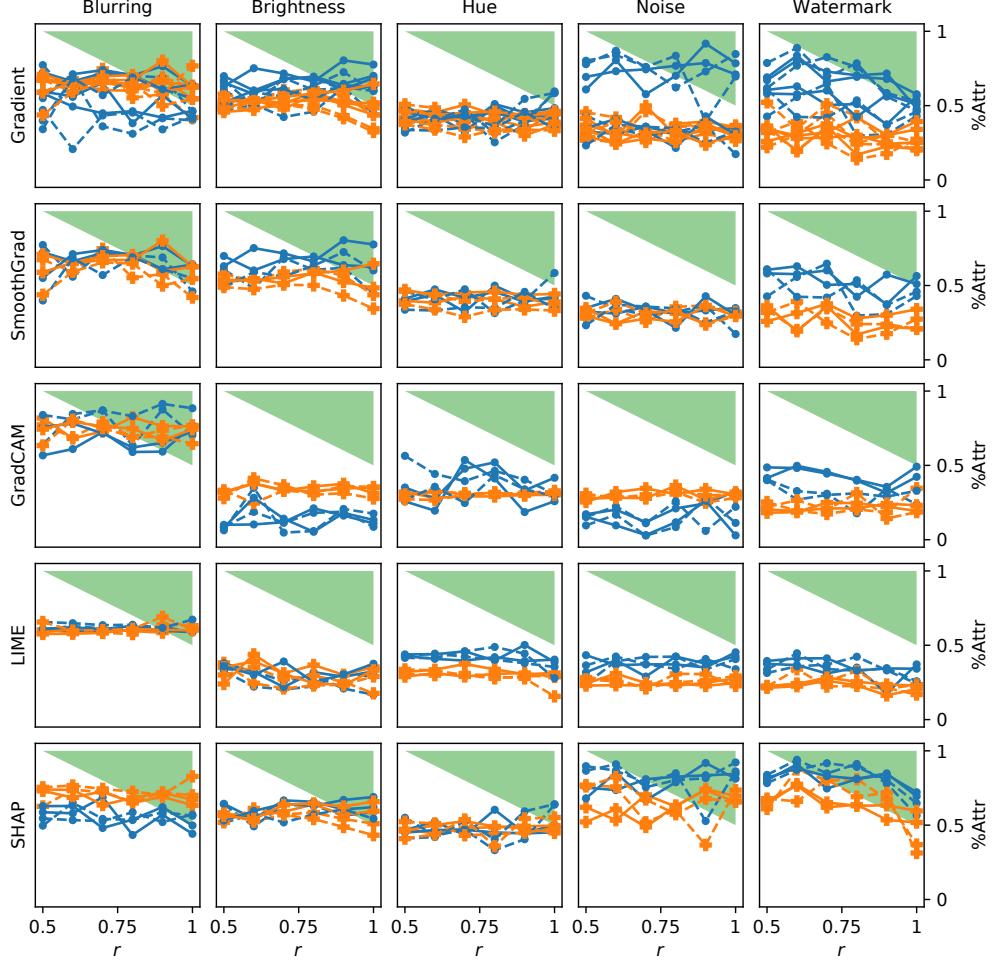

Figure 15: $\%\mathrm{Attr}$ vs label reassignment parameter r for all pairs of saliency maps and manipulations.

As explained in Sec. 5.4, $a(F)$ represents the expected accuracy of the model when given only feature F. Note that this value should *not* be calculated as the model accuracy on images with every pixel but F being blacked out, because such images are out of distribution where the model may exhibit unreasonable behaviors (similar to the discussion raised by Hooker et al. [11]).

Instead, the suppression of information beyond F can be understood as an inability for the model to distinguish inputs that agree on F. This leads to the following process of simulating such a prediction. First, let $\mathbb{P}_{X,Y|F=f}$ be the data distribution conditioned on $F = f$. Since all features other than F are suppressed, the model cannot further distinguish two inputs $x, x' \sim \mathbb{P}_{X|F=f}$. As a result, the expected accuracy can be computed by comparing the model's prediction on x against the ground truth label on x'. Then we take the expectation of this accuracy according to different values of $f \sim \mathbb{P}_F$, where $\mathbb{P}_F$ is the marginal distribution of F. Formally, for the model prediction function $g : \mathcal{X} \to \mathcal{Y}$, we have

$$a(F) = \mathbb{E}_{f \sim \mathbb{P}_F} \left[\mathbb{E}_{x,y \sim \mathbb{P}_{X,Y|F=f}} \left[\mathbb{E}_{x',y' \sim \mathcal{P}_{X,Y|F=f}} \left[\mathbb{1}_{g(x)=y'} \right] \right] \right]. \tag{6}$$

With balanced label distribution, $a(\varnothing)$ means that the model has no information about the input, and thus the accuracy is 0.5.

On the other hand, $a(F_M \cup F_O)$ means that the model has full access to the input, and thus the accuracy is the normal model accuracy p.

In addition, we have $a(F_O) \leq r$, because the label reassignment weakens the correlation between F_O and the label.

Finally and somewhat counter-intuitively, the above definition also implies that $a(F_M) = a(F_M \cup F_O) = p$ for the following reason: since every $F_M = f_M$ is perfectly correlated with the label, all the data in $\mathbb{P}_{X,Y|F_M=f_M}$ have the same label and thus the non-identifiability of any two inputs x and x' does not additionally degrade the model performance. However, note that this result comes from the mechanical application of Shapley value calculation, which is a popular and *axiomatic* definition of attribution. Whether it is reasonable in light of this implication is beyond the scope of the paper.

A.6 Attribution vs. Test Accuracy

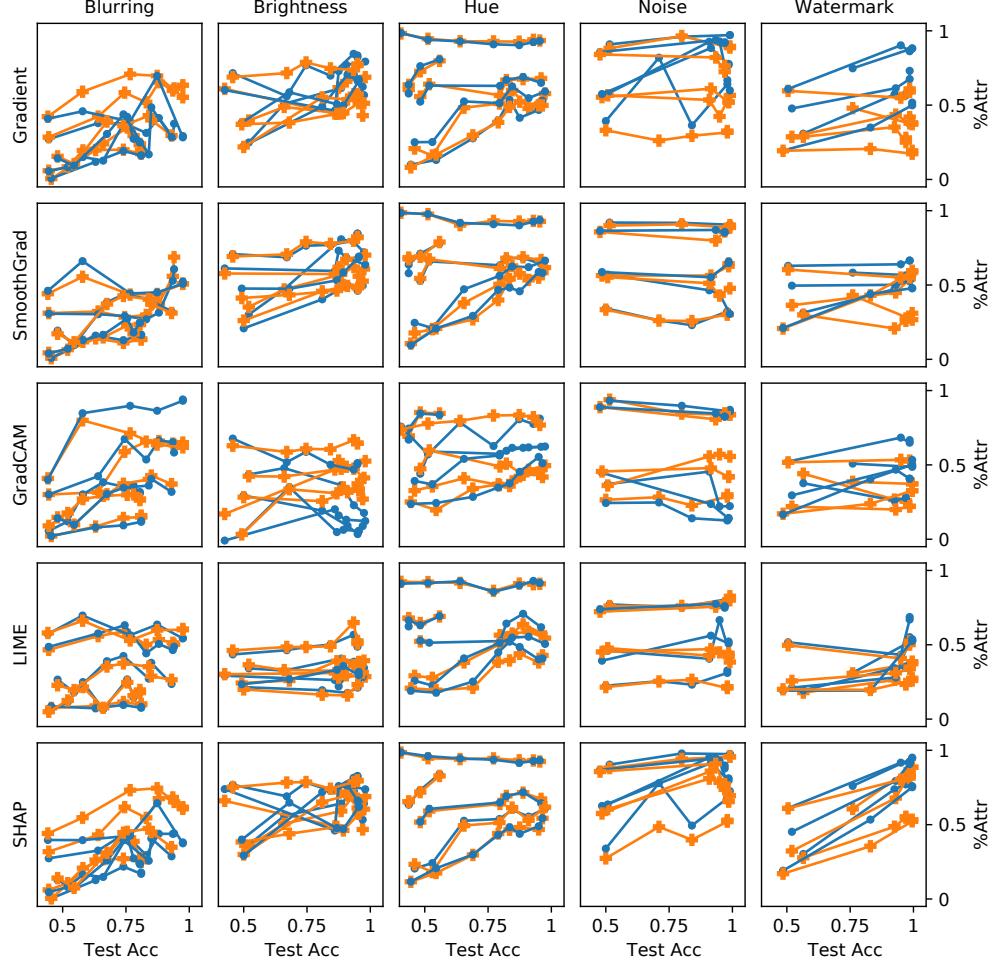Fig. 16 shows %Attr vs test accuracy for all pairs of saliency maps and manipulations.

Figure 16: %Attr vs test accuracy for all pairs of saliency maps and manipulations.

B Additional Details and Results for Attention Mechanism Evaluations

B.1 Model Architecture

The model architecture follows that described by Wiegreffe and Pinter [30] closely. First, a sentence of L words $(w_1, ..., w_L)$ is converted to a list of 200-dimensional embeddings $(\mathbf{v}_1, ..., \mathbf{v}_L)$ with the same embeddings used by Lei et al. [16] and Bastings et al. [6]. Then a Bi-LSTM network builds contextual representations for these words $\mathbf{h}_1, ...\mathbf{h}_L$, where $\mathbf{h}_i \in \mathbb{R}^{200}$ is the concatenation of the representation of the forward and the backward directions, each of 200 dimensions.

With $(\mathbf{h}_1, ..., \mathbf{h}_L)$, the attention mechanism computes the representation of the whole sentence $\mathbf{h}$ as

$$\mathbf{k}_i = \tanh(\text{Linear}(\mathbf{h}_i)) \in \mathbb{R}^{200}, \tag{7}$$

$$b_i = \mathbf{q} \cdot \mathbf{k}_i \tag{8}$$

$$a_1, ..., a_L = \text{softmax}(b_1, ..., b_L), \tag{9}$$

$$\mathbf{h} = \sum_{i=1}^{L} a_i \mathbf{h}_i, \tag{10}$$

where $\text{Linear}()$ represents a linear layer with learned parameters, $\mathbf{q} \in \mathbb{R}^{200}$ is a learned query vector applied to every sentence, and $a_1, ..., a_L$ are the attention weights for $w_1, ..., w_L$.

After the attention mechanism, a linear layer calculates the 2-dimensional logit vector, and the cross-entropy loss is used for gradient descent.

B.2 Highly Obvious Manipulations

Fig. 17 presents additional visualizations of the learned attention distribution of the model.
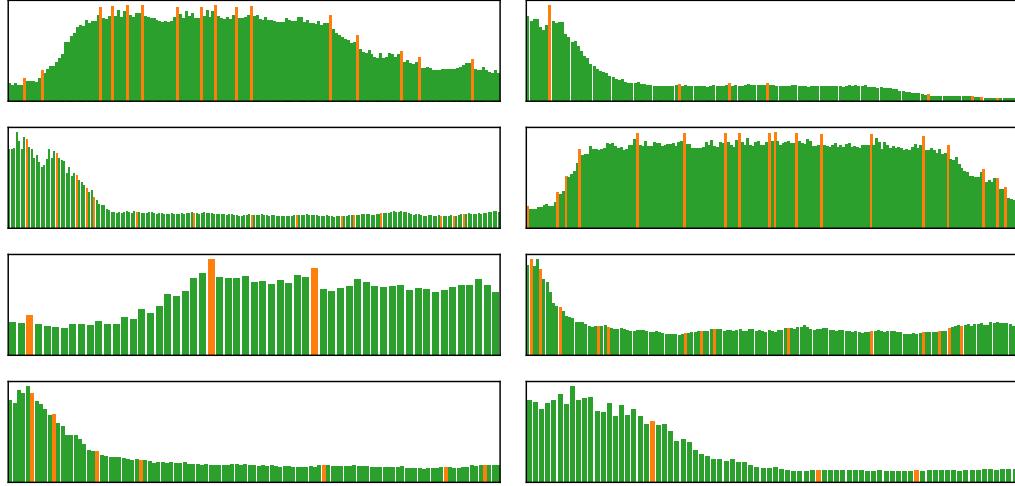

Figure 17: Additional attention distributions. Orange/green bars represent articles/non-articles.

B.3 Misleading Non-Correlating Features

Fig. 18 presents additional visualizations of the learned attention distribution on the *CN* (left) and *NC* (right) datasets.
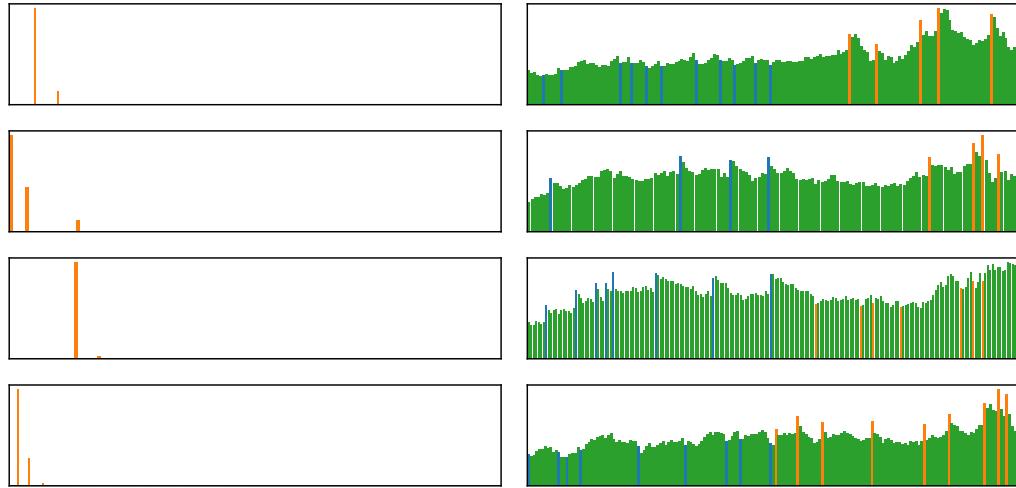

Figure 18: Additional attention visualizations on the *CN* (left) and *NC* (right) datasets. Orange/blue/green bars represent corr. articles/ non-corr. articles/other words.

C Additional Details and Results for Rationale Model Evaluations

C.1 Highly Obvious Manipulations

Fig. 19 presents four additional reviews annotated by the "faulty" CR model showing that it consistently selects the first few words of the review.

pours **a** clear yellow . 1/4 inch head of **a** white color . slight retention and slight lacing . smells of sweet malt , pale malt , fruit , and slight bread aroma . fits *a* style of **a** belgian pale ale . mouth feel is smooth and crisp with *a* high carbonation level . tastes of pale malt , yeast cleanliness , slight hops , and very slight fruit . overall , *a* decent brew but nothing special .	*bottle to* snifter glass . pitch black with little lacing around edge . smells like *the* typical oatmeal stout . taste has *the* great balance between both milk and oatmeal . sweet from *the* sugars and mild dark chocolate in *the* after taste . smooth and chewey . leans to *the* heavier side in *the* mouth . great example of two styles blended . worth seeking .
12oz can poured *into* pint glass . pours **the** pale golden straw color with **the** 2 finger fizzy head that settles quickly . slightly hazy when held to **the** light . smell is fairly nuetral with *the* bit of sweet malts coming through . *the* slight scent of something metallic . taste is decent . nothing crazy or unique but extremely clean , classic american pale lager flavor . mild light malt flavor with just enough hops for balance . no major off-flavors here . mouthfeel is fluid and crisp . this went down quickly and i am not **the** fizzy yellow beer fan . for what it is , it 's done well .	*a- dark* brown with hints of amber at **a** edges , small head which disappeared quickly and dissipated into **a** few sad bubbles . s- tons of sweet bourbon booze . raisins , sugared malts , dark chocolate filled with raspberry . t- booze and brown sugared malts mingle with one another . this is drinking like *a* barleywine to me . lots of wood and oak flavor drenched in booze . m- smooth creamy with enough carbonation . d- it 's *a* delicious brew that needs to be savored one of **a** best if not **a** best scotch ales ive had .

Figure 19: 4 additional reviews annotated by the "faulty" continuous relaxation model that consistently selects the first few words regardless. Selected non-articles in *orange bold italics*, selected articles in **green bold**, and missed articles in *red italics*.

C.2 Misleading Non-Correlating Features

Fig. 20 shows rationale selections by the two models for the same review at the same target %Sel.

	CN Dataset	NC Dataset
CR Model	enjoyed @ la cave **a** bulles ; simon & **a** head brewer of brasserie de vines hosted **a** tasting on 11/5 . medium body , frothy mouth-feel , nice carbonation . nice fruity notes upfront , green apples and citrus , with *the* hint of sourness . finishes with *the* fresh piney hop presence and *the* mild bitterness . overall ; great diversity in flavors , very fresh tasting .	enjoyed @ la cave *the* bulles ; simon & *the* head brewer of brasserie de vines hosted *the* tasting on 11/5 . medium body , frothy mouth-feel , nice carbonation . nice fruity notes upfront , green apples and citrus , with **a** hint of sourness . finishes with **a** fresh piney hop presence and **a** mild bitterness . overall ; great diversity in flavors , very fresh tasting .
RL Model	enjoyed @ la cave **a** bulles ; simon & **a** head brewer of brasserie de vines hosted **a** tasting on 11/5 . medium body , frothy mouth-feel , nice carbonation . nice fruity notes upfront , green apples and citrus , with *the* hint of sourness . finishes with *the* fresh piney hop presence and *the* mild bitterness . overall ; great diversity in flavors , very fresh tasting .	enjoyed @ la cave *the* bulles ; simon & *the* head brewer of brasserie de vines hosted *the* tasting on 11/5 . medium body , frothy mouth-feel , nice carbonation . nice fruity notes upfront , green apples and citrus , with **a** hint of sourness . finishes with **a** fresh piney hop presence and **a** mild bitterness . overall ; great diversity in flavors , very fresh tasting .

Figure 20: Additional reviews from *CN* and *NC* datasets for the two models. Selected words are underlined. Ground truth correlating articles are in **green bold**, and non-correlating articles in *red italics*. The CR model performs well on this review, focusing exclusively on correlating articles, while the RL model selects non-correlating articles, and misses a correlating one for the *NC* dataset.